

period oscillations in both devices, although the period  $\Delta V_g$  is approximately doubled in the 250- versus 500-nm QD. Because  $\Delta V_g$  is inversely proportional to the gate capacitance,  $\Delta V_g = e/C_g$ , and QD size, this comparison shows that the true size of the confined QD can be controlled in a predictable manner in these modulation-doped nanowires (22).

The potential of our approach for encoding coupled quantum structures has been explored in modulation-doped silicon nanowires that have structures of the form  $n^+-n_1-n_{\text{QD}}^+-n_2-n_{\text{QD}}^+-n_1-n^+$ , where  $n_1$  are fixed-width tunnel barriers that weakly couple the structure to source and drain electrodes, and  $n_2$  is a variable-width barrier that couples the two QDs (Fig. 4D, left panel). The  $I - V_g$  data recorded from representative nanowire devices with three different  $n_2$  barrier widths coupling the QDs (Fig. 4D, right panel) demonstrate several key points. First, the device with the largest barrier exhibits a single Coulomb oscillation period that yields a capacitance consistent with the size of each individual QD determined from SGM measurements. This result shows qualitatively that the two QDs are weakly coupled, and moreover, have sizes that are similar. Second, the data from the device with an intermediate-width  $n_2$  barrier exhibits a splitting of each of the Coulomb oscillation peaks into doublets, which is the signature of enhanced tunneling conductance between the QDs (23, 24). This observation agrees with previous studies (23, 25, 26) where coupled dots were defined by lithographically patterned gate electrodes. Last, as the barrier width is reduced further, a single Coulomb oscillation period is again observed, although the capacitance shows that the effective QD size is twice that of the individual  $n_{\text{QD}}^+$  regions; that is, the structures are fully delocalized.

These studies demonstrate the ability to synthesize coupled QDs within nanowires, where the interaction between quantum structures is defined by synthesis not lithography. More generally, this work demonstrates the potential of encoding functional information into nanostructures during synthesis, which we believe will open up opportunities for conventional and quantum electronic devices and circuits in the future.

#### Reference and Notes

1. P. L. McEuen, M. S. Fuhrer, H. Park, *IEEE Trans. Nanotechnology* **1**, 78 (2002).
2. H. Dai, *Acc. Chem. Res.* **35**, 1035 (2002).
3. C. M. Lieber, *Mater. Res. Soc. Bull.* **28**, 486 (2003).
4. L. Samuelson et al., *Phys. E* **25**, 313 (2004).
5. T. Mokari, E. Rothenberg, I. Popov, R. Costi, U. Banin, *Science* **304**, 1787 (2004).
6. M. S. Gudixsen, L. J. Lauhon, J. Wang, D. C. Smith, C. M. Lieber, *Nature* **415**, 617 (2002).
7. M. T. Bjork et al., *Appl. Phys. Lett.* **80**, 1058 (2002).
8. M. T. Bjork et al., *Nano Lett.* **4**, 1621 (2004).
9. C. Zhou, J. Kong, E. Yenilmez, H. Dai, *Science* **290**, 1552 (2000).
10. V. Derycke, R. Martel, J. Appenzeller, Ph. Avouris, *Nano Lett.* **1**, 453 (2001).

11. A. B. Greytak, L. J. Lauhon, M. S. Gudixsen, C. M. Lieber, *Appl. Phys. Lett.* **84**, 4176 (2004).
12. L. J. Lauhon, M. S. Gudixsen, D. Wang, C. M. Lieber, *Nature* **420**, 57 (2002).
13. Materials and methods are available as supporting material on Science Online.
14. J. M. Jasinski, S. M. Gates, *Acc. Chem. Res.* **24**, 9 (1991).
15. R. T. White, R. L. Espino-Rios, D. S. Rogers, M. A. Ring, H. E. O'Neal, *Int. J. Chem. Kinet.* **17**, 1029 (1985).
16. A. Bachtold et al., *Phys. Rev. Lett.* **84**, 6082 (2000).
17. P. M. Fahey, P. B. Griffin, J. D. Plummer, *Rev. Mod. Phys.* **61**, 289 (1989).
18. Y. Wu et al., *Nano Lett.* **4**, 433 (2004).
19. Z. Zhong, D. Wang, Y. Cui, M. W. Bockrath, C. M. Lieber, *Science* **302**, 1377 (2003).
20. A. DeHon, P. Lincoln, J. E. Savage, *IEEE Trans. Nanotechnology* **2**, 165 (2003).
21. L. P. Kouwenhoven et al., in *Proceedings of Advanced Study Institute on Mesoscopic Electron Transport*, L. L. Sohn, L. P. Kouwenhoven, G. Schön, Eds. (Kluwer, Dordrecht, Netherlands, 1997).
22. Recent studies have demonstrated the formation of single quantum dots in InP/InAs composition-modulated nanowires, where InP is used to produce confining barriers for an InAs QD (8).
23. F. R. Waugh et al., *Phys. Rev. B* **53**, 1413 (1996).
24. The tunneling conductance for the strongly coupled QDs was estimated to be  $0.9 G_0$ , where  $G_0 = 2e^2/h$ ,  $e$  is the elementary charge, and  $h$  is Planck's constant, assuming that interdot capacitance is negligible compared with individual QD capacitances (23).
25. N. Mason, M. J. Biercuk, C. M. Marcus, *Science* **303**, 655 (2004).
26. C. Fasth, A. Fuhrer, M. T. Bjork, L. Samuelson, *Nano Lett.* **5**, 1487 (2005).
27. We thank H. Park and A. DeHon for discussion. C.M.L. acknowledges support of this work by the Defense Advanced Research Projects Agency.

#### Supporting Online Material

www.sciencemag.org/cgi/content/full/310/5752/1304/DC1  
Materials and Methods  
Fig. S1

12 August 2005; accepted 24 October 2005  
10.1126/science.1118798

## Super-Compressible Foamlike Carbon Nanotube Films

Anyuan Cao,<sup>1\*</sup> Pamela L. Dickrell,<sup>2</sup> W. Gregory Sawyer,<sup>2</sup> Mehرداد N. Ghasemi-Nejhad,<sup>1</sup> Pulickel M. Ajayan<sup>3\*</sup>

We report that freestanding films of vertically aligned carbon nanotubes exhibit super-compressible foamlike behavior. Under compression, the nanotubes collectively form zigzag buckles that can fully unfold to their original length upon load release. Compared with conventional low-density flexible foams, the nanotube films show much higher compressive strength, recovery rate, and sag factor, and the open-cell nature of the nanotube arrays gives excellent breathability. The nanotube films present a class of open-cell foam structures, consisting of well-arranged one-dimensional units (nanotube struts). The lightweight, highly resilient nanotube films may be useful as compliant and energy-absorbing coatings.

Structural foams (1, 2) have a variety of applications in modern society such as in construction, energy dissipation, cushioning, and packaging. Mechanical strength (compressive stress) and compressibility (strain) are two important factors that determine the performance and applications of foams; however, these two properties are of opposing nature. Increasing the volume of the cells (i.e., the void area) in a foam results in higher compressibility (up to 75%) but causes rapidly decreasing strength (2–4). For the foam at a fixed chemical composition, its modulus ( $E_f$ ) decreases with increasing relative cell volume ( $\phi$ ) as  $E_f = CE(1 - \phi)^2$ , where  $C$  is a constant (close to unity) and  $E$  is the cell edge

modulus (1). Metallic (e.g., Al) foams have higher compressive strength than polymeric foams, but the plastic deformation of cell structures results in little resilience upon load release (5). The elastic segments (struts) between adjacent cells form the architecture of a foam, and it is the bending and buckling of these struts that allows the foam to be compressed; the property of a strut (determined by its composition, geometry, and dimension) dictates the compressive behavior (6, 7).

A carbon nanotube (8, 9) is perhaps the best strut to make ultralight yet strong foams, considering its exceptional mechanical strength, low density, and high elasticity (10). In particular, the nanotube exhibits extreme structural flexibility (10–12) and can be repeatedly bent through large angles and strains without structural failure (13). The ability of nanotubes to adopt and switch between various buckled morphologies makes them capable of accommodating and sustaining large local strains while maintaining structural integrity (14, 15).

We show that vertically aligned nanotubes (16) form a highly resilient open-cell

<sup>1</sup>Department of Mechanical Engineering, University of Hawaii at Manoa, Honolulu, HI 96822, USA. <sup>2</sup>Department of Mechanical and Aerospace Engineering, University of Florida, Gainesville, FL 32611, USA. <sup>3</sup>Department of Materials Science and Engineering, Rensselaer Polytechnic Institute, Troy, NY 12180, USA.

\*To whom correspondence should be addressed. E-mail: anyuan@hawaii.edu (A.C.); ajayan@rpi.edu (P.M.A.)

foam system, with individual nanotubes acting as strong nanoscale struts and the internanotube space acting as interconnected open-air cells. Repeated compression tests showed that these nanotube struts can be squeezed to less than 15% of their free lengths by buckling and folding themselves like springs, collectively. After every cycle of compressive loading, the nanotubes unfold the buckles and recover to their near original lengths, resulting in a strong cushioning effect.

Vertically aligned, multiwalled nanotube arrays were produced by chemical vapor deposition (CVD), with ferrocene and xylene as the precursors (17). Freestanding nanotube films that peeled off from the substrate (with typical areas ranging from 0.5 to 2 cm<sup>2</sup>) were compressed along the film-thickness direction (along nanotube axis) (Fig. 1) at a set constant strain, repeatedly for thousands of cycles. Two nanotube films squeezed to 15% of their original thickness recovered fully at the end of each cycle (movies S1 and S2). The porosity of the (as-grown) nanotube films is ~87% (18), potentially allowing a large volume reduction (up to 85%) when compressed. The near-full thickness recovery lasted hundreds of cycles before we saw a small reduction in thickness (gap between the top of the film and the compression stage) (fig. S1); however, the gap was stabilized at <20% of the total film thickness even after 10,000 cycles. The nanotube film did not fracture, tear, or collapse under compression, but remained at a constant width during the cycles (fig. S1). Previous work on nanotube brushes indicated that the shear resilience of aligned nanotubes is high, because no shedding of nanotubes was observed when the brushes were swept over solid surfaces (19).

Nanotube film-thickness recovery (back to its original morphology) during the compression-release period happens very fast. The compression head was set to retreat at a speed of 120 mm/min (upper limit of the instrument), and the film was observed to follow the returning head closely until it reached its maximum height (movie S2). Therefore, the film expansion rate on recovery can be considered to be at least the same speed as the receding head (>120 mm/min, or 2000  $\mu\text{m}/\text{sec}$ ). This is much faster than the general recovery rate for conventional flexible foams and spongy structures, especially those made of polymers with viscoelasticity that prevents instantaneous recovery at large strain rates.

Scanning electron microscopy (SEM) images show that the thickness of compressed nanotube films (>1000 cycles) decreases from the original 860  $\mu\text{m}$  to around 720  $\mu\text{m}$ . There are also ordered wavelike folds along the nanotubes, which are formed across the film section and correspond to the uniform horizontal lines seen in low magnification (Fig. 2A). The SEM

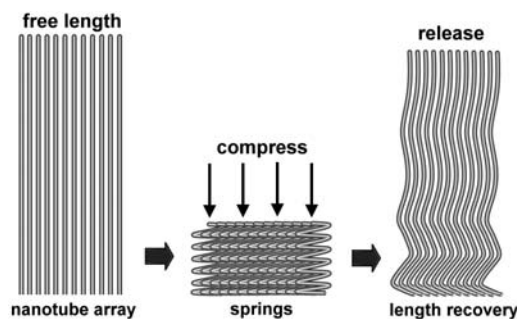


**Fig. 1.** Compression testing of aligned carbon nanotube films. A schematic illustration shows a nanotube array compressed to folded springs and then regaining the free length upon the release of compressive load.

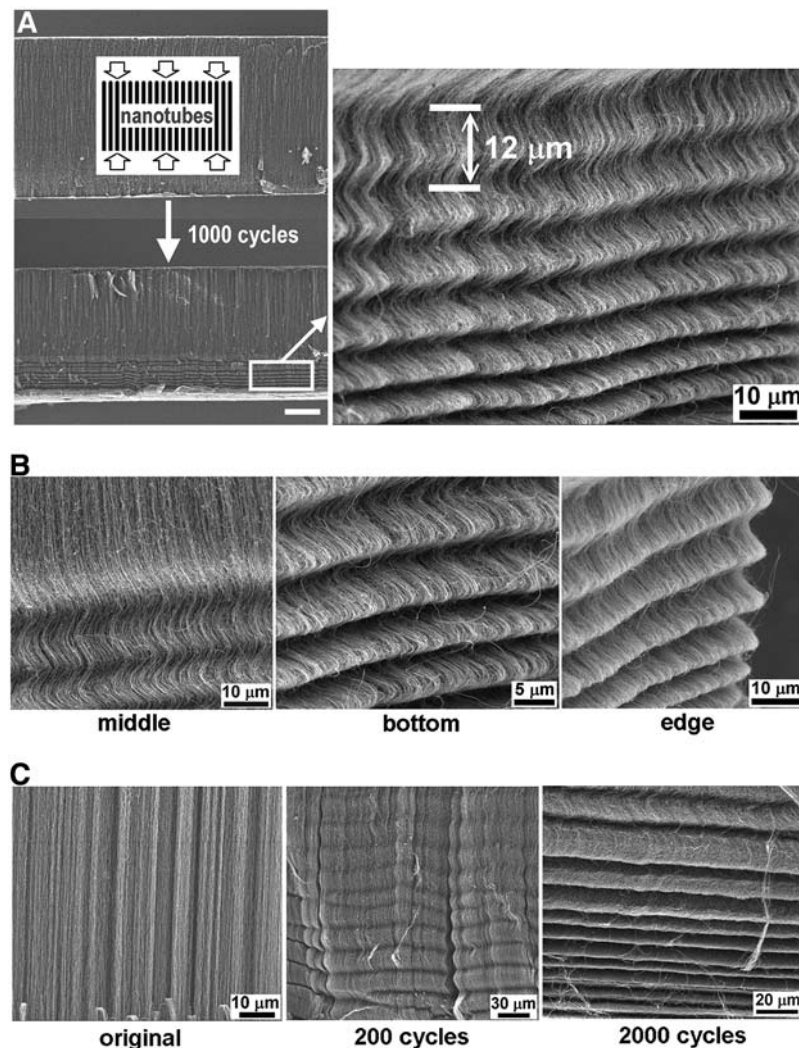


**Fig. 2.** SEM characterization of buckled carbon nanotubes under compression. (A) SEM of an original freestanding film (left, top) (thickness 860  $\mu\text{m}$ ) and a compressed film (left, bottom) ( $\epsilon = 85\%$ , 1000 cycles), with a reduced thickness of 720  $\mu\text{m}$ , showing horizontal lines (wavelike buckles) uniformly distributed across the film section. Left scale bar, 200  $\mu\text{m}$ . (Left, inset) Illustration of compression along the axis of nanotubes. (B) Slight buckles in the middle section, heavy buckles (almost completely folded) near the bottom of film, and the zigzag edge of the compressed film. (C) SEM image of a 1.2-mm-thick film before and after compression, showing the evolution of buckles with increasing compression cycles.

image shows that repeated compression has converted initially straight nanotubes into buckled folds, with an average wavelength of ~12  $\mu\text{m}$  (fig. S2). However, the buckles near the film's bottom side are heavily folded and

gradually released when approaching the middle part of the film, where the slight buckles are almost undistinguishable (Fig. 2B). The buckling wavelength increases with increasing original film thickness, with 25- $\mu\text{m}$  buckling

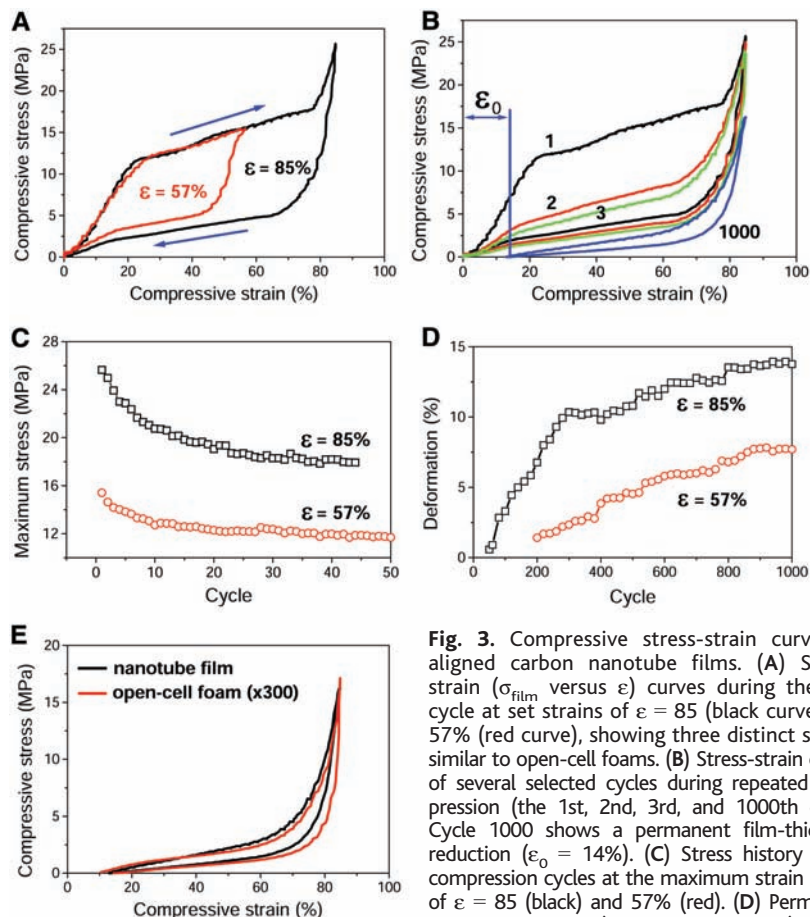


**Fig. 3.** Compressive stress-strain curves of aligned carbon nanotube films. (A) Stress-strain ( $\sigma_{\text{film}}$  versus  $\epsilon$ ) curves during the first cycle at set strains of  $\epsilon = 85\%$  (black curve) and  $57\%$  (red curve), showing three distinct stages, similar to open-cell foams. (B) Stress-strain curves of several selected cycles during repeated compression (the 1st, 2nd, 3rd, and 1000th cycle). Cycle 1000 shows a permanent film-thickness reduction ( $\epsilon_0 = 14\%$ ). (C) Stress history of 50 compression cycles at the maximum strain points of  $\epsilon = 85\%$  (black) and  $57\%$  (red). (D) Permanent film deformation (thickness reduction) occurs over 1000 compression cycles. (E) Stress-strain curves of a nanotube film (black) at cycle 1000 and an open-cell cushion foam (red) at cycle 10. The latter was multiplied by 300 for comparison.

over 1000 compression cycles. (E) Stress-strain curves of a nanotube film (black) at cycle 1000 and an open-cell cushion foam (red) at cycle 10. The latter was multiplied by 300.

for a 1.2-mm-thick film after compression. We still observe the same tendency to buckle more heavily at the bottom of the film (the side adjacent to the substrate during the growth of the films) (Fig. 2C). When the film is flipped during compression, the pattern also flips, with heavy folds appearing at the top, suggesting that the bottom of the film has slightly different mechanical characteristics (difference in density, stiffness) compared with the rest of the film (20). For an as-grown film consisting of nearly straight nanotubes, we observed slight buckles at the beginning compression cycles, which gradually became heavily folded after thousands of cycles (Fig. 2C). Because the buckles near the film bottom are always compressed earlier during each cycle, they are subjected to large-angle folding for a much longer time, compared with the buckles that develop later at the top portion of film. This time difference consequently aggravates the waviness difference observed here.

In a dense aligned nanotube array, it is difficult for nanotubes to buckle independently (randomly) at an appreciable length scale because of the proximity of the neighboring tubes. The cooperative nature of the buckling results in a self-organized, zigzag-folded mor-

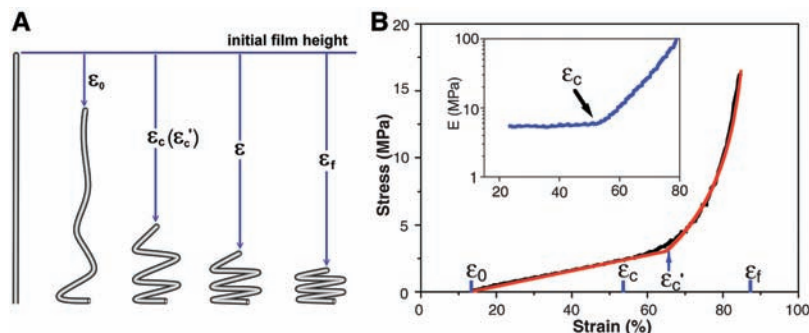
phology seen from the edge of the compressed film (Fig. 2B), which is the most space-efficient and energetically favorable configuration for huge numbers of nanotubes to adopt under large compressive strains. The folding of these zigzag buckles allows for the maximum volume reduction under the smallest compressive load and does not require any extra space to accommodate the vertical deformations.

Figure 3A shows the plots of compressive stress ( $\sigma_{\text{film}}$ , the applied force divided by the film area) versus strain ( $\epsilon$ , the compressed distance relative to film thickness) during the first compression cycle for the nanotube films (thickness  $\sim 860 \mu\text{m}$ ) at set maxima  $\epsilon$  of 57 and 85%. During the cycles, the stresses remain above zero until  $\epsilon = 0$ , in agreement with the full recovery of nanotube films from experimental observation. Three distinct stages are observed during the loading process, including an initial Hookean region at  $\epsilon < 22\%$  with an elastic modulus just over 50 MPa, a plateau (buckling of cell struts) at  $22\% < \epsilon < 79\%$  with a reduced modulus of approximately 12 MPa, and final densification, marked by rapid rise of stress as  $\epsilon$  approaches 85% (near monolith because of the large volume

reduction). Representative open-cell foams have shown similar three characteristic regions (5–7). Nanotube films subject to a moderate compression ( $\epsilon = 57\%$ ) show similar elastic behavior. The stress loops in both curves indicate that a large portion of energy (64%) is absorbed during compression. The energy dissipation is most likely caused by the friction between nanotubes (21) or movement of air through the porous nanotube arrays (which could be useful in damping applications).

Because nanotubes only occupy 13% of the film, the actual stress on each carbon nanotube ( $\sigma_{\text{cnt}}$ ) is several times higher than the as-measured film stress ( $\sigma_{\text{film}}$ ); that is,  $\sigma_{\text{cnt}} = \sigma_{\text{film}}/0.13 = 12 \text{ MPa}/0.13 = 92 \text{ MPa}$  at  $\epsilon = 22\%$ . Under Euler beam theory, the critical compression stress ( $\sigma_{\text{crit}}$ ) beyond which a nanotube strut becomes unstable (starts to buckle) can be expressed as  $\sigma_{\text{crit}} = E_{\text{CNT}}(\pi r/L_{\text{HW}})^2$ , where  $E_{\text{CNT}}$  denotes the Young's modulus of nanotubes,  $r$  is the nanotube radius (20 nm), and  $L_{\text{HW}}$  is the half wavelength of the buckle along nanotubes (15, 22). We used an average modulus of multiwalled nanotubes ( $E_{\text{CNT}}$ ) of 1 TPa, based on both experimental measurements and theoretical calculations (23–25). The critical stress necessary to enable the formation of 12- $\mu\text{m}$  buckles (half wavelength of 6  $\mu\text{m}$ ) as seen in Fig. 2A is  $\sigma_{\text{crit}} = 1 \text{ TPa} \times (\pi \cdot 20/6000)^2 = 110 \text{ MPa}$ , which is only slightly larger than the transition stress observed during the first loading curve ( $\sigma_{\text{cnt}} = 92 \text{ MPa}$ ). Thus we believe the nanotubes at first are subject to elastic bending and then form wavelike folds at  $\epsilon = 22\%$ , when the compressive stress is large enough to make them buckle collectively. The slightly lower critical stress for buckling may due to the structural defects in CVD-produced nanotubes. The Euler instability only permits a semiquantitative analysis on these naturally grown nanotube arrays. According to Hooke's law, the compression rate (force divided by displacement) of the whole film ( $R_{\text{film}}$ ) is determined by  $R_{\text{film}} = \sigma_{\text{film}}/\epsilon L$ , where  $L$  is the original film thickness (860  $\mu\text{m}$ ), and was calculated to be 26.5 kPa/ $\mu\text{m}$  at  $\epsilon < 79\%$ . Correspondingly, the compression rate of individual nanotubes ( $R_{\text{cnt}} = \sigma_{\text{cnt}}/\epsilon L$ ) with 12- $\mu\text{m}$  buckles is 204 kPa/ $\mu\text{m}$ .

Once the nanotubes have developed the self-organized folded patterns and have buckled collectively, the whole film becomes softer, which is seen by the loss of elasticity and decreased compressive stress in the cycles afterward (Fig. 3B), similar to the rapid stress decrease in the first several cycles of open-cell foams (26). The observed hysteresis is probably caused by the entanglement of nanotubes resulting in the impedance/friction during their movement. The stress at the maximum strain drops rapidly in the first 10 cycles (from 25.6 to 20 MPa at  $\epsilon = 85\%$ ) and then stabilizes at  $\sim 18 \text{ MPa}$  in the subsequent cycles (Fig. 3C).



**Fig. 4.** Modeling of nanotube behavior under large strain compression. (A) Illustration of nanotubes buckling under compression, where  $\epsilon_0$  is the permanent initial strain (14% at cycle 1000),  $\epsilon_c$  is the critical strain where the buckled nanotube folds begin to collapse from the bottom side,  $\epsilon$  is the strain relative to initial film, and  $\epsilon_f$  is the final strain where all folds are fully collapsed. (B) Experimental data of cycle 1000 (black curve) and the model (red curve) fit to this data. The experimental results show a critical strain ( $\epsilon_c$ ) of 53% from the differential curve (inset), whereas the model generates a critical strain ( $\epsilon_c'$ ) of 65%.

The maximum degradation in compressive strength of the nanotube film is <30% after 1000 cycles. The thickness reduction of the nanotube film can be derived from the intersection of stress curve with the strain coordinate ( $\epsilon_0 = 14\%$  for cycle 1000, as marked in Fig. 3B). For a repeated compression at a high strain of  $\epsilon = 85\%$ , the nanotube film shows high resistance to any further structural deformation, because the film height became subsequently stabilized at a deformation of <15% approaching 1000 cycles (Fig. 3D). Compression of films at smaller strains (e.g.,  $\epsilon = 57\%$ ) resulted in smaller thickness reduction ( $\sim 7.5\%$ ) after thousands of cycles.

The compressive strength (stress corresponding to the plateau region) of nanotube films (12 to 15 MPa) is much higher than typical low-density flexible foams that are capable of sustaining large strains (e.g., latex rubber, polyurethane), which generally have a plateau stress of only 20 to 30 kPa (3, 26). Measurements on several types of compressible foams and sponges (e.g., cushioning package foam, Gymboree, USA) revealed a maximum compressive stress of 0.02 to 0.1 MPa at a comparable strain ( $\sim 85\%$ ), which is two to three orders lower than the strength of nanotube films (Fig. 3E). The thickness deformation (which can't be recovered immediately) of such cushion foams is severe ( $>10\%$ ) within the first 10 cycles, and the thickness-regaining process is much slower (on the order of 1 mm/hour), compared with the fast unfolding rate of nanotubes ( $>2$  mm/min). The sag factor, which is the relative ratio of stresses at two deflections of 65 and 25%, is an important criteria for cushioning foams (26). This criteria represents how much "fight back" will be encountered upon continued compression. For nanotube films (at cycle 1000,  $\sigma = 3.55$  MPa at  $\epsilon = 65\%$  and  $\sigma = 0.84$  MPa at  $\epsilon = 25\%$ ), the sag factor is higher than 4. The resilience of nanotube films is 25 to 30%, measured by dropping a glass ball (1 to 2 mm

in diameter) from zero speed onto the film and calculating the ball rebound height relative to the initial ball-to-film distance before dropping. In addition, the open-cell nature of nanotube films also provides good breathability (allowing high-rate compression and recovery). The high compressive stress, sag factor, resilience, and breathability make nanotube films suitable for applications requiring strong cushioning effects.

Considering compression cycle 1000 shown in Fig. 3B, the derivative of its stress-strain curve depicts an initial linear elastic stage up to a critical strain  $\epsilon_c = 53\%$  (inset of Fig. 4B) with a single modulus of  $E = 5.85$  MPa, after which the modulus increases exponentially with increasing strain. The exponential increase in stiffness can be explained through a complete collapse of individual nanotube folds starting from the bottom of film, thus reducing the number of folds participating in further deformations, until all the folds have been fully compressed (corresponding to a final strain of  $\epsilon_f$ ) (Fig. 4A). The stress of the initial linear stage is  $\sigma = E(\epsilon - \epsilon_0)$ , and the second stage can be expressed differentially as  $d\sigma/d\epsilon = E/(\epsilon_f - \epsilon)$ . Figure 4B shows that the model featured by these two equations (red curve) fits quite well with the experimental data (black curve) of cycle 1000, yielding a critical strain of  $\epsilon_c' = 65\%$  (18). The earlier collapse of nanotube buckles ( $\epsilon_c = 53\%$ ) in experimental results is attributed to the mechanically weaker region of the film near the bottom surface of the film, where the heaviest buckles were observed in Fig. 2.

Carbon nanotube films behave as open-cell foams with nanotubes as elastic struts. The high compressibility ( $\sim 85\%$ ), recovery rate ( $>2000$   $\mu\text{m}/\text{sec}$ ), sag factor ( $\sim 4$ ), and fatigue resistance ( $<15\%$  deformation during thousands of cycles) make nanotube arrays/films potential foamlike structures with much improved strength/weight ratio, dimensional stability (at elevated temperature or humidity),

and resistance to chemical environments. Aligned single-walled nanotubes are expected to have better performance (strength, resilience). In addition, the compressive strength of nanotube films could be tailored by controlling the wavelength of buckles. Such resilient nanotube systems could have many applications, such as flexible electromechanical systems, compliant interconnect structures, actuators, and coatings for mechanical damping and energy-absorbing services.

## References and Notes

- L. J. Gibson, M. F. Ashby, *Cellular Solids, Structure and Properties* (Pergamon, New York, 1997).
- N. C. Hilyard, A. Cunningham, *Low Density Cellular Plastics, Physical Basis of Behavior* (Chapman and Hall, London, UK, 1994).
- D. Klemperer, K. C. Frisch, in *Handbook of Polymeric Foams and Foam Technology* (Hanser, New York, 1991), chaps. 4, 6, and 9.
- H. X. Zhu, J. F. Knott, N. J. Mills, *J. Mech. Phys. Solids* **45**, 319 (1997).
- L. J. Gibson, *Annu. Rev. Mater. Sci.* **30**, 191 (2000).
- J. H. Kinney, G. W. Marshall, S. J. Marshall, D. L. Haupt, *J. Appl. Poly. Sci.* **80**, 1746 (2001).
- H. X. Zhu, N. J. Mills, J. F. Knott, *J. Mech. Phys. Solids* **45**, 1875 (1997).
- M. S. Dresselhaus, G. Dresselhaus, P. C. Eklund, *Science of Fullerenes and Carbon Nanotubes* (Academic, San Diego, 1996).
- R. H. Baughman, A. A. Zakhidov, W. A. de Heer, *Science* **297**, 787 (2002).
- D. Qian, G. J. Wagner, W. K. Liu, M. F. Yu, R. S. Ruoff, *Appl. Mech. Rev.* **55**, 495 (2002).
- S. Iijima, C. Brabec, A. Maiti, J. Bernholc, *J. Chem. Phys.* **104**, 2089 (1996).
- V. Sazonova et al., *Nature* **431**, 284 (2004).
- M. R. Falvo et al., *Nature* **389**, 582 (1997).
- B. I. Yakobson, C. J. Brabec, J. Bernholc, *Phys. Rev. Lett.* **76**, 2511 (1996).
- O. Lourie, D. M. Cox, H. D. Wagner, *Phys. Rev. Lett.* **81**, 1638 (1998).
- Z. F. Ren et al., *Science* **282**, 1105 (1998).
- R. Andrews et al., *Chem. Phys. Lett.* **303**, 467 (1999).
- Materials and methods are available as supporting material on Science Online.
- A. Cao et al., *Nat. Mater.* **4**, 540 (2005).
- When we immersed a nanotube film in organic solvents (e.g., acetone) and then took it out, the condensed film after acetone evaporation was slightly curled toward the bottom side (more shrinkage near the bottom). Thus we believe that the bottom part of a film is less dense (strong), compared with its top part.
- J. Suhr, N. Koratkar, P. Keblinski, P. Ajayan, *Nat. Mater.* **4**, 134 (2005).
- S. Timoshenko, in *Theory of Elastic Stability* (McGraw-Hill, New York, 1936), chap. 2.
- M. M. J. Treacy, T. W. Ebbesen, J. M. Gibson, *Nature* **381**, 678 (1996).
- M. F. Yu et al., *Science* **287**, 637 (2000).
- J. P. Lu, *Phys. Rev. Lett.* **79**, 1297 (1997).
- N. C. Hilyard, in *Mechanics of Cellular Plastics* (Macmillan, New York, 1982), pp. 103 and 226.
- A.C. acknowledges the start-up funding from the College of Engineering and the Mechanical Engineering Department of the University of Hawaii at Manoa. P.M.A. thanks the Interconnect Focus Center New York.

## Supporting Online Material

www.sciencemag.org/cgi/content/full/310/5752/1307/DC1

Materials and Methods

Figs. S1 and S2

Movies S1 and S2

16 August 2005; accepted 21 October 2005  
10.1126/science.1118957